Single-Molecule van der Waals Compass

Xiao Chen (chenx123@tsinghua.edu.cn)
Tsinghua University https://orcid.org/0000-0003-1104-6146
Boyuan Shen
Tsinghua University
Huiqiu Wang
Tsinghua University
Hao Xiong
Tsinghua University
Weizhong Qian
Tsinghua University
Dali Cai
Tsinghua University
Shifeng Jin
Chinese Academy of Sciences
Xin Liu
Dalian University of Technique
Yu Han
King Abdullah University of Science and Technology
Fei Wei
Tsinghua University

Research Article

Keywords: molecule, van der Waals, interactions, porous material, molecular imaging

DOI: https://doi.org/10.21203/rs.3.rs-61856/v1

Abstract

Imaging the single molecules is always challenging under the diverse microscopes, but highly demanded for investigating the intermolecular interactions at the molecular level1-6. The van der Waals (vdW) interactions at sub-nanometer scale will deeply influence various molecular behaviors under the confinement conditions7-11. Here, inspired by the traditional compass12, we introduce a classical strategy using a vertical para-xylene (PX) molecule as a rotating pointer to detect the vdW potential field in a MFI straight channel. Based on the integrated differential phase contrast scanning transmission electron microscopy (iDPC-STEM)13-17, we achieve the real-space imaging of single PX molecule pointer in each channel with a certain orientation. The solid relation between the pointer orientation and atomic channel structure in this vdW compass is established by combining the calculations and imaging results. Thus, these PX orientations help us identify the varied vdW potential field related to the channel geometry both in the spatial and temporal dimensions. This work not only provides a visible and sensitive pointer to investigate the host-guest vdW interactions in porous materials at the molecular level, but also promotes the further imaging and study of other single-molecule behaviors by the iDPC-STEM.

Main Text

Compass, one of the most ancient artificial tools recorded both in Chinese and western historical materials[12], has played an important role in the process of human development and exploration. In a normal compass, a magnetized pointer could orient itself roughly north-south showing the pole direction of geomagnetic field, which may be the earliest principle used to measure the distribution of electromagnetic field. Over decades, it is still challenging to achieve the detection of smaller-scale interactions between atoms and molecules under the guidance of such classical principles. The *van der Waals* (vdW) interactions, between the neutral and polarizable atoms, molecules or particles, are ubiquitous in various physical, chemical and biological processes across different scales[18,19]. However, the direct measurements of vdW force usually involved various sophisticated nanotechniques[20-22] difficult to be extended to more complex multi-atoms systems. For example, the vdW potentials in nanoscale channels determine various physical and chemical behaviors of confined molecules, such as sorption, transport, catalysis and phase transition[7-11], but they are still a great challenge to investigate at the single-molecule level with current methods. Analogous to the principle of traditional compass, we can introduce a rotating molecular pointer with the defined direction marks into the channels. And, the orientations of rotating pointers will reveal the spatial vdW potentials in the surrounding circumstances, if they can be precisely identified.

Directly observing the molecular configurations helps us better understand the interactions at the atomic scale[1-6]. And, in the compass-analogy strategy for detecting the vdW potentials, the single-molecule imaging of compass construction is also highly demanded to identify the exact pointer orientations. However, it still requires very advanced imaging techniques to ‘see’ the real single molecules, especially the small organic molecules, due to the its high instability and sensitivity to electrons. Recently, an

emergent imaging mode, the integrated differential phase contrast (iDPC) scanning transmission electron microscopy (STEM)[13-15], brings us new possibility to observe small organic molecules. The iDPC-STEM has been proved to be an efficient tool for imaging the beam-sensitive materials with ultra-high resolution and signal-to-noise ratio, and the contrasts of light elements are enhanced in the iDPC-STEM images[16,17]. These advantages allow the iDPC-STEM to be considered as an efficient tool to image and investigate the single-molecule behaviors in the real-space.

In this work, we establish a nanoscale vdW compass with single para-xylene (PX) molecule as a pointer confined in the straight channels of quasi-2D MFI-type frameworks[23,24]. According to the orientations of the rotating PX pointers, we can identify the vdW interactions between the PXs and surrounding Si/O atoms. And, using the Cs-corrected iDPC-STEM, we image not only the atomic structures of the MFI-type channels but also the single PX molecule in each channel with ultimate resolution. We find the imaged orientation of PX pointer is closely related to the channel geometry and the corresponding vdW potential field in each channel. Then, we observe the rotation of PX pointer in response to the channel deformations both in the spatial and temporal dimensions. These results provide a compass-inspired strategy to detect the vdW interactions under the confinement of nanochannels using a rotating pointer, which will help us investigate various single-molecule behaviors in the sorption, transport, catalysis and phase transition.

The MFI-type framework owns a cross-linked channel system consisting of straight and sinusoidal channels, which can be imaged from the [010] and [100] projections respectively (Fig. S1 and S2). Inspired by the reconstruction of traditional compass in Fig. 1a, we used the single PX molecule as a rotating pointer and the Si_{10}/O_{10} ring of MFI straight channel as direction marks to construct our vdW compass in Fig. 1b and c. The elliptical Si_{10}/O_{10} ring is numbered to indicate 20 discrete directions about 18° apart. And, such straight channel (with the size of ~5.6×5.3 Å) can just contain only one C_6-ring (with the kinetic diameter of ~5.8 Å) as a size-matched pointer. Based on the previous adsorption studies in MFI-type zeolites[25-31], monocyclic aromatics can be stably confined at the intersections of the straight and sinusoidal channels, and their long molecular axes are nearly parallel to the straight channel (b-axis of MFI framework). Then, the aromatic pointer will show an energetically preferred orientation due to the vdW interaction with surrounding Si/O atoms, and rotate with the change of channel geometry to detect the different vdW potential fields inside the channels as it does in a traditional compass.

The quasi-2D MFI-type zeolites we used in this work are derived from the short-b-axis ZSM-5 (a typical MFI-type zeolite) nanocrystals[16] (Fig. S3). In Fig. 1d, the annular dark field (ADF) STEM image from the [010] projection shows the shape of short-b-axis ZSM-5 with a smooth (010) surface. After etched by the sodium carbonate (Na_2CO_3), the ZSM-5 nanocrystals own a hollow shape with very thin (quasi-2D) areas as shown in Fig. 1e and Fig. S4. The corresponding intensity profile in Fig. 1f indicates the different contrasts due to a wide range of thicknesses. The pristine ZSM-5 crystals (thick areas) are uniformly 30-50 nm thick, while the etched parts (thin area) are estimated to show a thickness less than 5 nm. From the lateral view (the [100] projection), the ADF-STEM image and profile analysis in Fig. 1g and h indicate

the thickness of the thinnest areas in the etched ZSM-5 can be reduced to 2~3 nm, which is nearly the thickness of single unit cell in the b-axis direction. And, in the magnified image (Fig. 1i), we obtain the lateral view of the quasi-2D ZSM-5 lattice, where each straight channel has complete intersection with only one sinusoidal channel as a stable adsorption site of PX molecule. These results confirm that the quasi-2D ZSM-5 area for the single-molecule imaging is successfully built by this etching method. Then, at this quasi-2D area, the iDPC-STEM helps us resolve the atomic structure of MFI-type framework from the [010] projection. As shown in Fig. 1j, the projected positions of Si atoms and the arrangement of empty straight channels can be clearly displayed, which are highly consistent with the inset structural model.

Then, PX molecules were adsorbed into the straight channels of ZSM-5 directly from the PX liquid phase as the pointers of vdW compass. And, we imaged an etched ZSM-5 crystal adsorbing PXs, the shape and thickness of which are shown in the ADF-STEM image and corresponding intensity profile in Fig. 2a and b. Fig. 2c and d are the iDPC-STEM image and the intensity profile of the thick area (marked by the blue frame), while Fig. 2e and f are those of the thin area (marked by the cyan frame). After the PX filling, we can clearly observe the oriented spindle-shaped spots in these channels compared to the empty ZSM-5 framework in Fig. 1j. And, their orientations (more obvious in the thick area) can be directly identified in the iDPC-STEM images, which are required for detecting the interactions in the vdW compass. In the profiles in Fig. 2d and f, we normalized the intensities from 0 to 1 to quantitatively compare these profiles in different images. And, the black dash line is the normalized profile of the empty channels, and the red line is the normalized profile of the PX-filling channels. The adsorbed PX molecules can be expressed by the small peaks in the valleys of empty channels.

Moreover, the intensity profiles of the thick and thin areas are a little different. In the thick area, the PX spots in channels represent the arrays of PX columns, not the single molecules. Thus, the number of PX molecules in each channel is naturally varied when the PX adsorption isn't saturated. As we observed in Fig. 2d, the intensities of PX peaks, which are related to the numbers of PX molecules in channels, are varied as marked by a wide red band. However, in the intensity profile of the thin area in Fig. 2f, the intensities of PX peaks keep constant in these channels, since there will be only one intersection site for the PX adsorption within 2 nm thickness. Furthermore, we calculated the projected electrostatic potentials as the simulated image from the [010] projection (Fig. 2g). The simulation is conducted using the structural model with one PX molecule in single unit cell and based on the same parameters with the iDPC-STEM imaging. And, in Fig. 2f, the blue dash line is the normalized intensity profile of the simulated image. We find that the intensities of the PX peaks in the iDPC-STEM and simulated images are highly consistent. These results also confirmed, in another way, that the thickness of the etched ZSM-5 crystal was reduced to about 2 nm and we have imaged the single PX molecule in each channel.

To further study the relation between the PX orientations and host-guest interactions, we detailedly checked the magnified iDPC-STEM images of individual channels with different PX orientations. Fig. 3a shows the iDPC-STEM image of an empty ZSM-5 channel. After the PX filling, there is a spindle-shaped spot indicating a vertical PX molecule which appears in the dark channel as shown in Fig. 3b. The red

arrow shows the orientation of PX molecule, which points to the O-2 direction as defined in Fig. 1c. In this image, we can identify the exact positions of ten Si atoms around the channel as marked by the blue dots. More accurately, we used the intensity profiles to measure the projected distances of opposite Si atoms in Fig. S5 and Table S1. Then, we fixed the positions of Si atoms (the distances of opposite Si atoms) and optimized the structure of single MFI unit cell. And, we calculated the energetically preferred configuration in this unit cell based on the density functional theory (DFT) method. Fig. 3c gives the channel geometry and PX configuration with the most optimal energy corresponding to Fig. 3b. The PX pointer in this vdW compass points out the vdW potential field from by the surrounding atoms along the O-2/O-7 direction.

Moreover, in Fig. 3d-f, the iDPC-STEM images show other three PX orientations in different MFI channels. We did the same image processing and structural optimization based on the channels in these images, and then, calculated the theoretical configurations of inside PX pointers as shown in Fig. S6. It is obvious that the channel geometry is totally different in each channel. And, these calculated results are all highly consistent with the imaging results, where the PX pointers point to the Si-1, Si-2 and O-3 in Fig. 3d-f respectively. Meanwhile, we also calculated the energies of PX molecules with different orientations in the channel models obtained from these four images. In each channel model, we rotated the PX molecules so that it pointed to the atoms O-1, Si-1, O-2, Si-2, O-3 and Si-3 respectively. The results are summarized in Fig. 3g, and the imaged orientation indeed shows the lowest energy as we expected. The energy difference between the adjacent PX orientations is about 0.04-0.12 eV. Based on the Boltzmann distribution laws, the most stable configuration occurs with about 5-100 times probability of the adjacent ones in the dwell time of probe scanning (16 μs), which, thus, can be finally reflected in the images. These calculations reveal that the imaged orientation of PX pointer is closely related to the channel geometry and the corresponding vdW potential field inside the channels. That is, we firstly noticed the aperiodicity in the ZSM-5 framework by the real-space iDPC-STEM imaging with the atomic resolution, which leads to the varied host-guest vdW interaction in each channel. Such different vdW interactions, especially their directions, can be directly detected by the imaged (most probable) orientations of every PX pointers analogous to the principle of traditional compass.

The above analysis of single iDPC-STEM image reveals the spatial distribution of vdW potential field in each channel on the 2D [010] projection. Next, we continuously took several images of the same region to study the varied orientations of PX pointer in temporal dimension. Fortunately, we clearly captured the single-molecule orientation changing in a same channel from these continuous images (Fig. 4a-f and Fig. S7). Due to the time-consuming probe scanning and image integration processes of iDPC-STEM, the time interval for these images is about 1-2 minutes. The changes in this time scale do not result from the thermal vibrations of the framework and molecules, but the shift of equilibrium configuration due to the changing channel geometry. As shown in Fig. S8, the profile analysis reveals that this channel was clearly deformed when continuously imaged. Based on the mechanism of electron beam damage[xx], the framework deformation may be induced by the locally accumulated charging and heating under a long-time irradiation. Then, in Fig. 4g, the red data points indicate the change of PX orientation, while the blue

data points provide the distances between the opposite atoms Si-1 and Si-6 in these images, which are the most volatile data in Fig. S8. We find that the trends of these two sets of data points are highly consistent. That is, the PX orientation changes in response to the channel deformation and points out the resulting change of vdW potential field in this channel. These results accord with the conclusion about the relation between the channel geometry and pointer orientation we derived from Fig. 3. And, the imaged rotation of PX pointer further prove the availability of using compass-analogy strategy to real-time detect the time-variant channel geometry and corresponding vdW potential field inside.

In summary, the unique structure of a single-molecule vdW compass, consisting of a MFI-type straight channel and a PX pointer inside, can be directly resolved by the iDPC-STEM. Especially, the configuration of single PX molecule can be identified in the iDPC-STEM images to detect the host-guest vdW interactions in the MFI-type frameworks. That is, we directly 'see' the orientations of PX pointers in these channels, making the strategy based on the single-molecule vdW compass possible to be applied to the detection of molecular interactions in a confined space. For example, the PX pointer provides both the spatial distribution and the real-time change of the vdW potential field in each channel, proving the availability of this strategy in the PX/ZSM-5 system. Moreover, achieving the single-molecule imaging under various microscopes is always a milestone in the nanotechnology and molecular science. The iDPC-STEM help us real-space image single organic molecules in porous materials for the first time. And other organic molecules, such as homologues of aromatics, can also be confined and imaged in MFI and other size-matching porous frameworks. Thus, this work may provide a general method to investigate the host-guest interactions in a series of organic/inorganic systems by direct imaging, which have attracted wide research interests in the sorption and catalysis, however, difficult to be studied at the molecular level. Such progress on the imaging technique will promote the further study on the physical and chemical properties of guest molecules, and bring new insights into diverse single-molecule behaviors.

Methods

Synthesis of quasi-2D ZSM-5 crystals

First, the short-b-axis ZSM-5 crystals we used were synthesized via a hydrothermal method. The tetrapropylammonium hydroxide (TPAOH) was used as the template. The silicon source was the tetraethyl orthosilicate (TEOS), and the aluminum source was the $Al(NO_3)_3$•$9H_2O$. In a typical synthesis, 13.1 g TPAOH, 11.2 g TEOS, 2.0 g urea, 0.3 g $Al(NO_3)_3$·$9H_2O$, 0.1 g NaOH and 0.1 g iso-propanol (IPA) were added into 18.4 g H_2O under stirring. After being stirred for 1-2 h at room temperature, the gel was transferred into a Teflon-lined autoclave for temperature-programming crystallization. The crystallization temperature was heated from room temperature to 180 °C with a rate of 15 °C/h, and then hold on for 48 h. Subsequently, the crystallization was quenched by cold water. The product was filtered, washed, dried at 110 °C in air, then calcined at 550 ℃ for 5 h to remove the remaining organic template.

Then, the obtained Na-ZSM-5 were further etched by 1 M Na_2CO_3 solution at 80 °C for 24 h. In this step, the hollow shapes of some ZSM-5 crystals are formed showing the quasi-2D areas with near single-unit-

cell thickness due to the dissolution of silica. The resulting crystals were separated by filtration and washed for three times, subsequently dried at 110 °C in air. Finally, the obtained sample was converted into the H-ZSM-5 by three ion exchanges with 1 M NH_4NO_3 solution and subsequent calcination in air at 550 °C for 5 h.

Filling PX in ZSM-5 framework

PX molecules were absorbed into ZSM-5 straight channels directly from the liquid phase. Some ZSM-5 powder and pure PX liquid were added into a 1-mL centrifuge tube. The ZSM-5 crystals were dispersed in PX liquid using ultrasound for 30 min. The centrifuge tube was stored for a period of time to fully diffuse the PX molecules into the ZSM-5 frameworks. And before the STEM observations, the specimens were dispersed using ultrasound for another 30 min to image the separated ZSM-5 crystals.

The iDPC-STEM imaging

The iDPC-STEM and ADF-STEM observations were performed using a Cs-corrected STEM (FEI Titan Cubed Themis G2 300) operated at 300 kV with convergence semi-angle of 10 mrad. The microscope was equipped with a DCOR+ spherical aberration corrector for the electron probe which was aligned before experiments using a standard gold sample. The following aberration coefficients were measured as: A1=1.41 nm; A2= 11.5 nm; B2=22.2 nm; C3=2.05 μm; A3=525 nm; S3=177 nm; A4=8.81 μm, D4=2.39 μm, B4=13.2 μm, C5=-3.95mm, A5=295 μm, S5=111μm, and R5=102 μm assuring a 60 pm resolution under normal circumstances. The beam current employed for the iDPC-STEM is lower than 0.1 pA. The collection angle of the iDPC-STEM is 4-20 mrad. The iDPC-STEM is a direct phase imaging mode, which is linear in the phase shift of transmission function and the projected electrostatic potential in a thin sample. Thus, we used the mapping of the projected electrostatic potential as the simulated images, which was simulated by the QSTEM software based on the multislice method. The parameters for simulations, such as the convergence angle, collection angle and resulting resolution, were selected to be as same as those in our imaging experiments.

The first-principles-based calculations

All the periodic first-principles-based calculations are based on density functional theory (DFT) and were carried out by using the Perdew-Burke-Ernzerhof (PBE) exchange-correlation functional within the generalized gradient approach (GGA) as implemented in the Vienna Ab initio Simulation Package (VASP)[32,33]. The projected augmented wave (PAW) formalism are used to consider the effect of the core and valence electrons in the valence density[34], the valence electrons were described by plane wave basis sets with a cut-off energy of 400 eV. Gamma points were used for Brillouin zone integration. The vdW dispersion interaction between the PX molecule and the zeolite was considered using the DFT-D3 scheme[35,36]. The energy and force convergence criteria were 1.0×10^{-5} eV and 0.03 eV·Å^{-1} in all calculations. The single unit cell (a = 20.022, b = 19.899 and c = 13.383 Å) containing 96 Si atoms and 192 O atoms was used to represent the MFI-type lattice.

Then, the channel geometry was optimized based on the imaging results. The projected distances between the opposite Si atoms in four channels in Fig. 3 are summarized in Table S1. We modified the projected distances between opposite Si atoms to match those measured in the imaging results, and then fixed them during the further optimization. After that, the adjusted MFI unit cell was fully optimized, and all atoms except the fixed Si atoms were relaxed until the forces are smaller than 0.03 eV·Å^{-1}. To optimize the configuration of PX molecule in the channel, we put a PX molecule at the intersection of two types of channels (straight and sinusoidal channels). Then, the orientation of confined PX and the geometry of MFI framework were fully optimized with all atoms except the fixed Si atoms were relaxed until the forces are smaller than 0.03 eV·Å^{-1}. Simultaneously, the energy of optimized MFI framework with confined PX molecule (the most probable configuration) was calculated. After that, other sub-optimized PX orientations within four optimized channels are obtained by rotating the PX molecule along the b-axis of MFI-type framework. And, the MFI-type frameworks with different sub-optimized PX orientations were respectively used to perform single point energy calculation.

Data availability

All the data are available in the online version of the paper. The data that support the findings of this study are available from the corresponding authors on reasonable request.

Declarations

Acknowledgments:

This work was supported by the National Key Research and Development Program of China (2018YFB0604801), the National Basic Research Program of China (973 Program, 2011CB932602), the National Natural Science Foundation of China (No.20141301065 and 21306103).

References

1. J. Lee, W. Ho, Single-bond formation and characterization with a scanning tunneling microscope. *Science* **286**, 1719-1722 (1999).
2. M. A. Lantz et al., Quantitative measurement of short-range chemical bonding forces. *Science* **291**, 2580-2583 (2001).
3. L. Gross, F. Mohn, N. Moll, P. Liljeroth, G. Meyer, The chemical structure of a molecule resolved by atomic force microscopy. *Science* **325**, 1110-1114 (2009).
4. B. J. Albers et al., Three-dimensional imaging of short-range chemical forces with picometre resolution. *Nat. Nanotech.* **4**, 307-310 (2009).

5. L. Gross et al., Organic structure determination using atomic-resolution scanning probe microscopy. *Nat. Chem.* **2**, 821-825 (2010).
6. J. Zhang et al., Real-Space Identification of Intermolecular Bonding with Atomic Force Microscopy. *Science* **342**, 611-614 (2013).
7. M. Eddaoudi et al., Systematic design of pore size and functionality in isoreticular MOFs and their application in methane storage. *Science* **295**, 469-472 (2002).
8. Z. Lai et al., Microstructural optimization of a zeolite membrane for organic vapor separation. *Science* **300**, 456-460 (2003).
9. N. L. Rosi et al., Hydrogen storage in microporous metal-organic frameworks. *Science* **300**, 1127-1129 (2003).
10. J. R. Li, R.J. Kuppler, H. C. Zhou, Selective gas adsorption and separation in metal–organic frameworks. *Chem. Soc. Rev.* **38**, 1477-1504 (2009).
11. P. J. Bereciartua et al., Control of zeolite framework flexibility and pore topology for separation of ethane and ethylene. *Science* **358**, 1068-1071 (2017).
12. J. B. Carlson, Lodestone compass - Chinese or Olmec primacy. *Science* **189**, 753-760 (1975).
13. H. Rose, Nonstandard imaging methods in electron microscopy. *Ultramicroscopy* **2**, 251-267 (1977).
14. I. Lazic, E. G. T. Bosch, S. Lazar, Phase contrast STEM for thin samples: Integrated differential phase contrast. *Ultramicroscopy* **160**, 265-280 (2016).
15. E. Yucelen, I. Lazic, E. G. T. Bosch, Phase contrast scanning transmission electron microscopy imaging of light and heavy atoms at the limit of contrast and resolution. *Sci. Rep.* **8**, 1-10 (2018).
16. B. Shen et al., Atomic spatial and temporal imaging of local structures and light elements inside zeolite frameworks. *Adv. Mater.* **32**, 1906103 (2020).
17. B. Shen, X. Chen, K. Shen, H. Xiong, F. Wei, Imaging the node-linker coordination in the bulk and local structures of metal-organic frameworks. *Nat. Commun.* doi:10.1038/s41467-020-16531-y (2020).
18. Margenau, H. Van der Waals forces. *Rev. Mod. Phys.* **11**, 1–35 (1939).
19. Israelachvili, J. N. Intermolecular and surface forces (*Academic Press*, 2011).
20. S. V. Aradhya, M. Frei, M. S. Hybertsen, L. Venkataraman, Van der Waals interactions at metal/organic interfaces at the single-molecule level. *Nat. Mater.* **11**, 872-876 (2012).
21. L. Beguin, A. Vernier, R. Chicireanu, T. Lahaye, A. Browaeys, Direct measurement of the van der Waals interaction between two Rydberg atoms. *Phys. Rev. Lett.* **110**, 263201 (2013).
22. S. Kawai et al., Van der Waals interactions and the limits of isolated atom models at interfaces. *Nat. Comm.* **7**, 11559 (2016).
23. E. M. Flanigen et al., Silicalite, a new hydrophobic crystalline silica molecular sieve. *Nature* **271**, 512-516 (1978).
24. G. T. Kokotailo, S. L. Lawton, D. H. Olson, W. M. Meier, Structure of synthetic zeolite ZSM-5. *Nature* **272**, 437-438 (1978).

25. H. Van Koningsveld, F. Tuinstra, H. Van Bekkum, J. C. Jansen, The location of p-xylene in a single crystal of zeolite H-ZSM-5 with a new, sorbate-induced, orthorhombic framework symmetry. *Acta Cryst.* **B45**, 423-431 (1989).
26. R. Goyal, A. N. Fitch, H. Jobic, Powder neutron and X-ray diffraction studies of benzene adsorbed in zeolite ZSM-5. *J. Phys. Chem. B* **104**, 2878-2884 (2000).
27. J. C. Taylor, Hexadeuteriobenzene locations in the cavities of ZSM-5 zeolite by powder neutron diffraction. *J. Chem. Soc. Chem. Commun.* **15**, 1186-1187 (1987).
28. C. A. Fyfe, J. S. J. Lee, L. M. D. Cranswick, I. Swainson, Powder neutron diffraction determination of the structure of the o-xylene/zeolite ZSM-5 complex. *Micropor. Mesopor. Mater.* **112**, 299-307 (2008).
29. C. A. Fyfe, D. H. Brouwer, Optimization, standardization, and testing of a new NMR method for the determination of zeolite host-organic guest crystal structures. *J. Am. Chem. Soc.* **128**, 11860-11871 (2006).
30. C. A. Fyfe, A. C. Diaz, H. Grondey, A. R. Lewis, H. Forster, Solid state NMR method for the determination of 3D zeolite framework/sorbate structures: $^{1}H/^{29}Si$ CP MAS NMR study of the high-loaded form of p-xylene in ZSM-5 and determination of the unknown structure of the low-loaded form. *J. Am. Chem. Soc.* **127**, 7543-7558 (2005).
31. B. Boronat, A. Corma, What is measured when measuring acidity in zeolites with probe molecules? *ACS Catal.* **9**, 1539-1548 (2019).
32. J. P. Perdew, K. Burke, M. Ernzerhof, Generalized gradient approximation made simple. *Phys. Rev. Lett.* **77**, 3865-3868 (1996).
33. G. Kresse, J. Furthmüller, Efficient iterative schemes for ab initio total-energy calculations using a plane-wave basis set. *Phys. Rev. B* **54**, 11169-11186 (1996).
34. P. E. Blöchl, Projector augmented-wave method. *Phys. Rev. B* **50**, 17953-17979 (1994).
35. S. Grimme, Accurate description of van der Waals complexes by density functional theory including empirical corrections. *J. Comput. Chem.* **25**, 1463-1473 (2004).
36. S. Grimme, Semiempirical GGA-type density functional constructed with a long-range dispersion correction. *J. Comput. Chem.* 2006, **27**, 1787-1799 (2006).

Figures

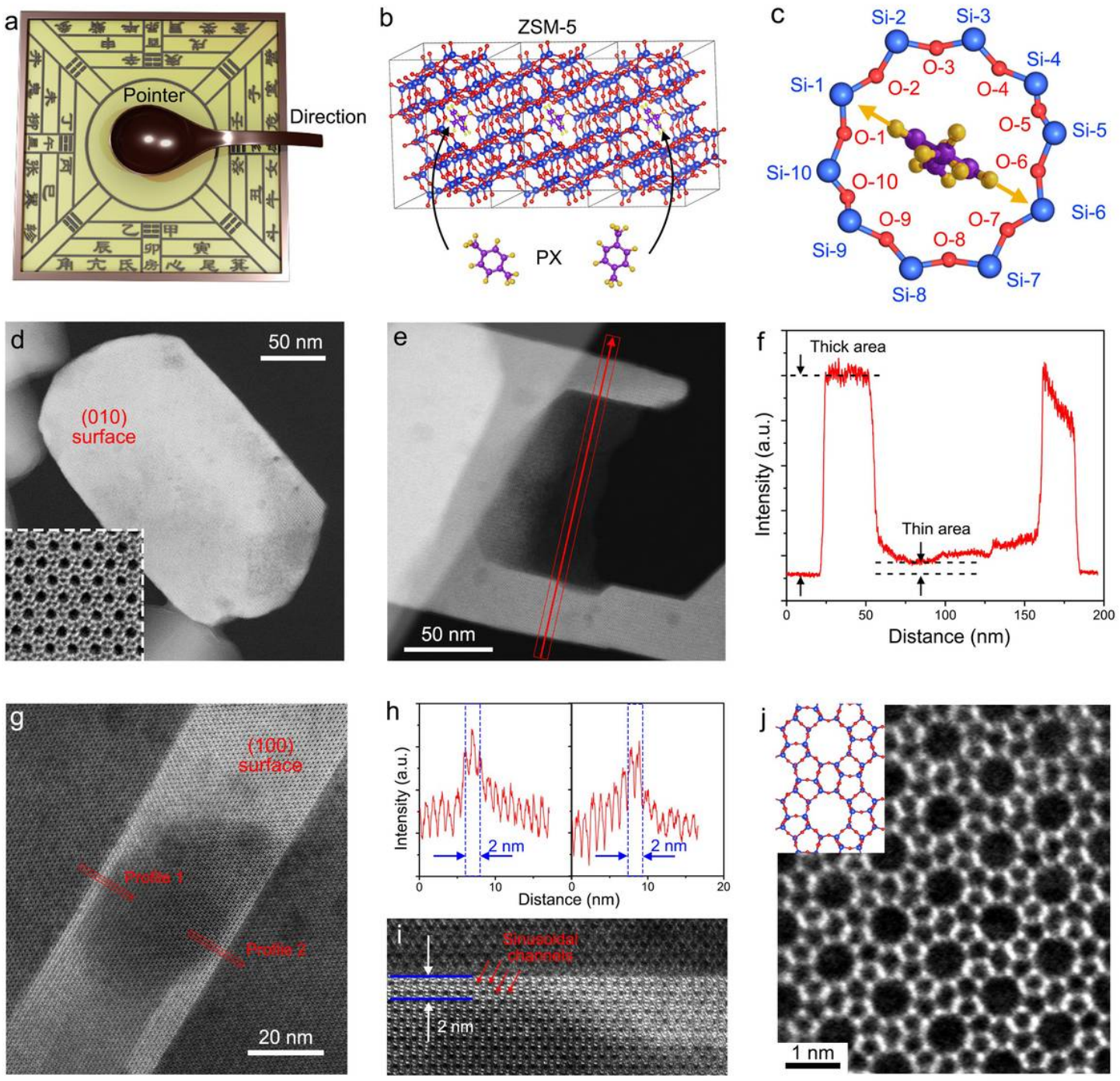

Figure 1

Quasi-2D ZSM-5 frameworks for single-molecule vdW compass. a, The reconstruction of a traditional Chinese compass. b, Making a single-molecule vdW compass by filling ZSM-5 channels with PX molecules. c, The projected structure of the single-molecule vdW compass with a PX pointer in a numbered Si10/O10-ring. d, The ADF-STEM image showing the shape of a short-b-axis ZSM-5 crystal. The straight channels can be imaged from this [010] projection. e,f, The ADF-STEM image (e) and the corresponding profile analysis (f) of an etched ZSM-5 crystal with an obvious quasi-2D thin area from the [010] projection. g,h, The ADF-STEM image (g) and the corresponding profile analysis (h) of an etched

ZSM-5 crystal from the lateral view (the [100] projection) indicating the 2~3-nm thickness of the thinnest areas. i, The magnified ADF-STEM image of this etched ZSM-5 crystal showing the lateral lattice of quasi-2D ZSM-5 area where the sinusoidal channels can be clearly imaged. j, The atomic iDPC-STEM image and the structural model (inset) of the empty ZSM-5 framework from the [010] projection.

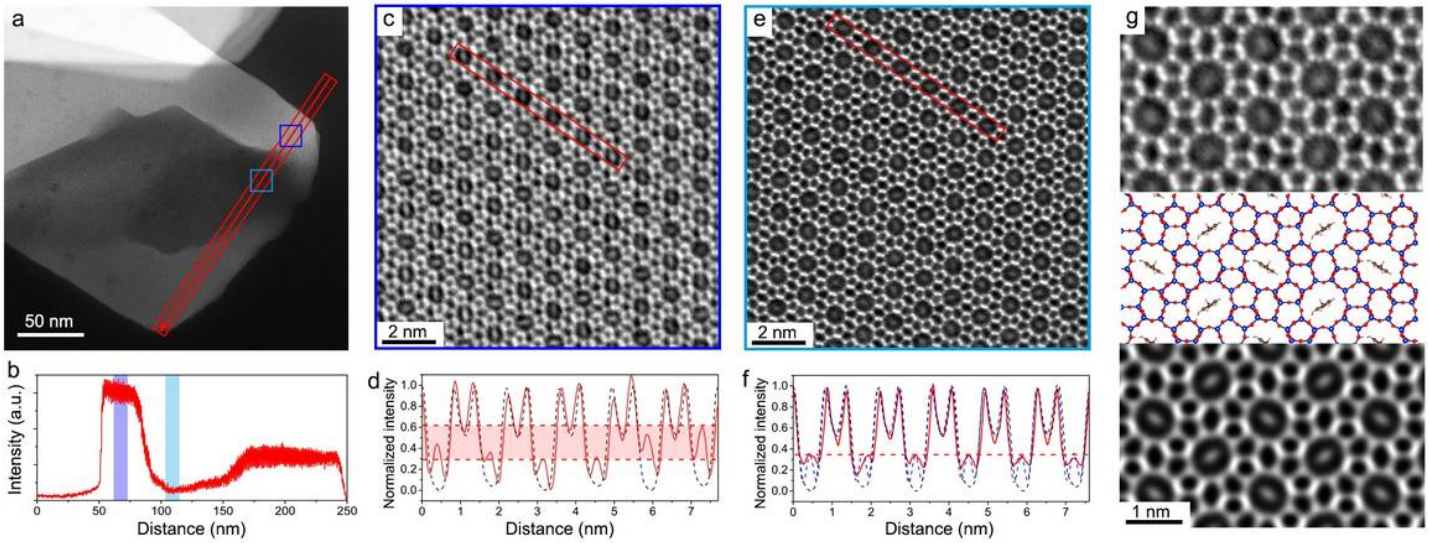

Figure 2

Imaging the oriented PX molecules in ZSM-5 straight channels. a,b, The ADF-STEM image (a) and the corresponding profile analysis (b) of a etched ZSM-5 crystal after the PX-filling. c,d, The iDPC-STEM image (c) and the corresponding profile analysis (d) of a thick area in ZSM-5 crystal. In these profiles, the red line is the normalized intensity profile of the thick PX-filling ZSM-5 as marked in c, while the black dash line is that of the empty ZSM-5. e,f, The iDPC-STEM image (e) and the profile analysis (f) of a thin area (about single-unit-cell thickness) in ZSM-5 crystal. In these profiles, the red line is the normalized intensity profile of the thin PX-filling ZSM-5 as marked in e, while the black and blue dash lines are those of the empty ZSM-5 and the simulated result with only single PX molecule respectively. g, The comparison between the magnified iDPC-STEM image (top), the structural model (middle) and the simulated projected electrostatic potentials (bottom) of the 2D ZSM-5 with single PX molecule in each straight channel.

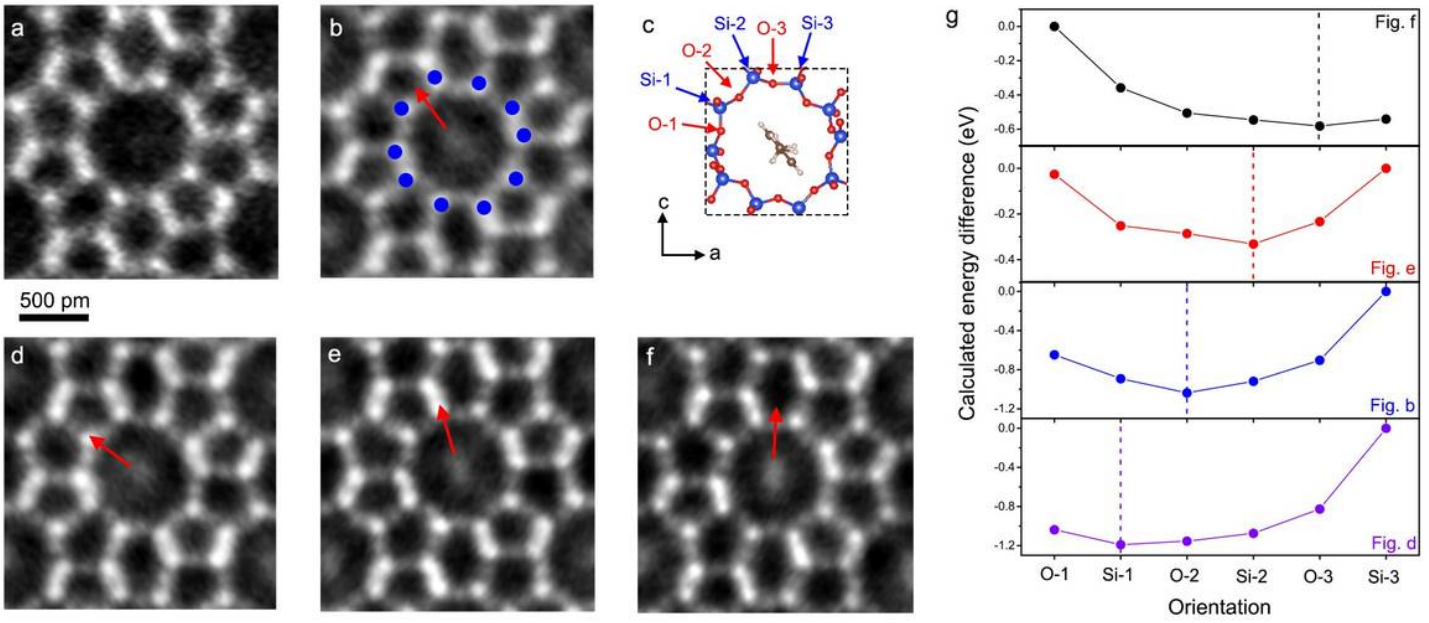

Figure 3

Identifying the varied orientations of PX pointers. a, The magnified iDPC-STEM image of an empty straight channel. b, The magnified iDPC-STEM image of a PX-filling straight channel. The red arrow indicates the PX orientation pointing to the atom O-2. c, The optimized channel geometry and the inside PX configuration calculated according to the measured Si atom positions in b. d-f, The magnified iDPC-STEM images with other three PX orientations marked by the red arrows. g, The calculated energy differences of PX pointers at different orientations in the channel models optimized according to the structures in b, d, e, f respectively.

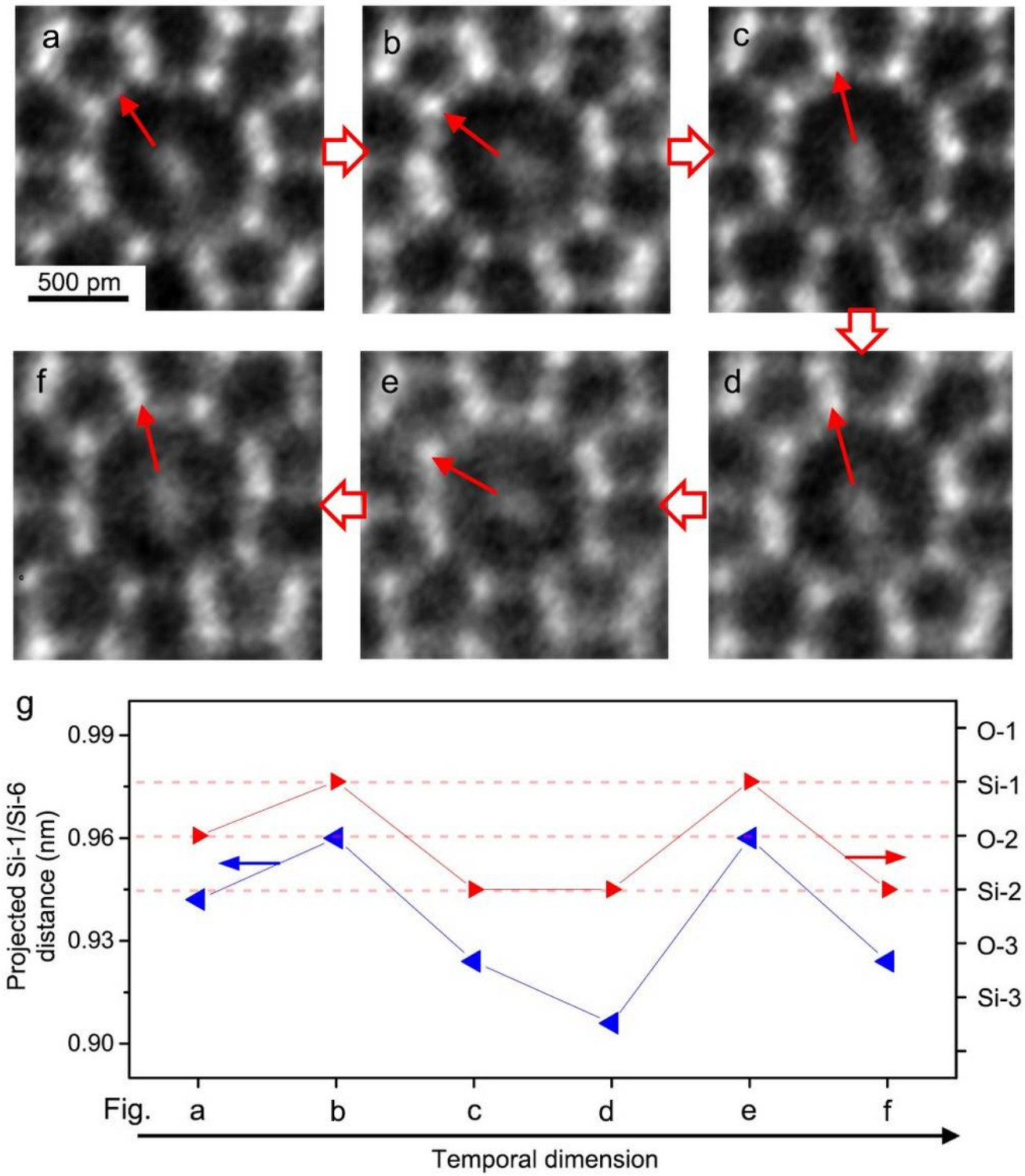

Figure 4

The time-variant orientation of PX pointer dependent on the changing channel geometry. a-f, The magnified iDPC-STEM images of a same PX-filling channel continuously captured from the same area. The red arrows show the time-variant orientation of PX pointer in this channel. g, The synchronous changes of PX orientation and channel geometry in different images. The red data points show the PX

orientations changing with time, while the blue data points show the corresponding Si-1/Si-6 distances in these images measured by the profile analysis.

Supplementary Files

This is a list of supplementary files associated with this preprint. Click to download.

- 3824630supp3493933qhhchj.pdf